Desalination and Water Treatment
www.deswater.com
doi: 10.5004/dwt.2019.24655

169 (2019) 209–221
November

Preparation and adsorption properties of iron and manganese modified N-doping mesoporous carbon from waste biomass

Yi Chen[a], Shuang Zhang[a], Min Wang[a], Wenju Jiang[a,b], Ruzhen Xie[a], Lu Yao[a,b], Xia Jiang[a,b,*]

[a]*College of Architecture and Environment, Sichuan University, Chengdu 610065, China, Tel. +86-28-85467800; Fax: +86-28-85405613; emails: xjiang@scu.edu.cn (X. Jiang), 1040712646@qq.com (Y. Chen), 1016524224@qq.com (S. Zhang), 412144769@qq.com (M. Wang), wenjujiang@scu.edu.cn (W. Jiang), xieruzhen@scu.edu.com (R. Xie), yaolu@scu.edu.cn (L. Yao)*
[b]*National Engineering Research Center for Flue Gas Desulfurization, Chengdu 610065, China*

Received 24 March 2019; Accepted 30 June 2019

ABSTRACT

The iron and manganese modified mesoporous carbon (MC-Fe, MC-Mn and MC-Fe/Mn) was prepared from waste biomass with nitrogen-doping assistance. The modified MCs were characterized by BET, XRD, Fourier transform infrared spectrometry and X-ray photoelectron spectroscopy, respectively. It was found that the introduction of nitrogen on MCs restrained the pore plugging caused by metals doping, and its BET surface area and total pores volume were around 1,200 m^2/g and 1.00 cm^3/g, respectively, because nitrogen could facilitate the dispersion of metals on MC evenly. The introduction of Fe might promote the formation of –O–CH_3 while Mn might contribute to the formation of the C=O functional group on the surface of MCs. The adsorption results show that the adsorption capacities of modified MCs toward methylene blue (MB) were enhanced evidently by the introduction of Fe and/or Mn, which was increased from 911 to 1,030 mg/g. The higher adsorption capacity of MB could be attributed to the unchanged porous structure, metal active adsorption sites and modified surface chemistry on modified MCs.

Keywords: Mesoporous carbon; Waste biomass; Iron; Manganese; Adsorption

1. Introduction

A large quantity of dye wastewater has been released into water body from textile and leather industry. The dyes are hard to be degraded by microorganism in water due to the organic ingredients, and some ingredients of dyes also have the biological toxicity [1], which is against the growth of aquatic organisms and destroys the ecological balance. Various methods have been reported to remove dyes from water, such as biodegradation [2], catalytic oxidation [3] and adsorption [4,5]. The adsorption is widely applied due to the high efficiency and low cost. Activated carbon (AC) is considered as one of the most ideal adsorbents due to the developed porosity and abundant surface functional groups [4,5].

Pore structure is one of the most important factors which influence the adsorption properties of AC. Micropores can only adsorb and separate micro molecule, while mesopores can adsorb relatively larger molecules such as dyes and biomacromolecules [6]. Mesoporous carbon (MC) with the pore size distribution range of 2–50 nm possesses a great adsorption capacity for dyes such as methylene blue (MB), due to the fact that MB molecules can easily diffuse into mesopores [7].

MC is usually prepared by hard template method using pure organic agents such as phenol, resorcinol and phloroglucinol as carbon precursors and silicon substrate as

* Corresponding author.

templates, while it is necessary to use hydrofluoric acid (HF) to wash the templates [8,9]. However, HF is highly corrosive and not environmental friendly, and the cost of pure organic agents also is very high [8]. Recent years, the waste biomass such as sawdust is used as the raw material of AC [10], which could decrease the cost greatly, together with the reutilization of organic waste. In addition, the MC enriched with mesopores can also be obtained from waste biomass using phosphoric acid as the activation agent through the reaction with carbon to form mesopores during heating process [7,11]. In the meantime, phosphoric acid could help dehydration and crosslinking of biopolymers such as cellulose, hemicellulose and lignin in biomass, thereby obtaining a high yield of carbon [7]. Thus, it is environmental friendly and inexpensive to obtain MC from waste biomass by phosphoric acid activation.

In order to enhance the adsorption performance of MC, metal oxides are usually introduced, which could change the surface functional groups and surface charge, leading to a better adsorption performance [12–14]. Transition metals such as Fe and Mn have been mostly used due to the low cost and high efficiency. Meanwhile, magnetic materials would be advantageous to those based on biomass or agricultural byproducts, which can exhibit similar capacities, based on simple activation procedures such as impregnation and calcination. It was found that the Fe-doped AC showed the increased potential for the removal of MB [14]. Both Fe and Mn-doped AC can greatly enhance the removal of MB from aqueous solution [12,15]. The introduction of Fe and Mn may cause the change in oxygen-containing functional groups to facilitate the adsorption [12,14,15]. However, it was found that the specific surface area and total pore volume of the metals doped carbon reduced greatly, possibly because the metal oxides nanoparticles tend to agglomerate, blocking the carbon pores [13].

Recently, it was found that nitrogen-doped AC could improve the adsorption performance of metal ions, due to the adsorption and complexation of metal ions by nitrogen-containing groups [16,17]. It was found that the carbon aerogel enhanced greatly the removal of Cr(VI) and Pb(II) through nitrogen doping [17]. It was reported that magnetic nitrogen-doped porous carbon composites exhibited good chemical stability and adsorption capacity [16]. Therefore, it is possible that the introduction of metal ions on nitrogen-doped carbon might help facilitate uniform dispersion of metal particles on carbon surface to reduce the agglomeration of metal ions. In addition, MC could be an ideal support to immobilize metals due to its large pore volume, high specific surface area, large and controllable pore size. It was found that the nano Fe^0 immobilized on MC could overcome the drawbacks of Fe^0 aggregated [18]. However, very few studies had been found on the preparation of metal modified MC by nitrogen-doped assistance for the adsorption of dyes wastewater.

Thus, the purpose and the novelty of this study were to prepare Fe and Mn modified nitrogen-doped MC for the removal of dyes. The pore structure and surface chemical properties of the modified carbon were characterized, and their adsorption performance toward MB was investigated. Finally, the adsorption isotherms and kinetics were also studied to investigate their adsorption mechanisms.

2. Materials and methods

2.1. Materials

The raw material of activated carbon was cypress sawdust, which was obtained from the furniture factory in Guangyuan, Sichuan. The urea, ferric nitrate nonahydrate $Fe(NO_3)_3{\cdot}9H_2O$, 50% Mn nitrate solution $Mn(NO_3)_2$ and MB trihydrate were purchased from Chengdu Chron Chemicals (Chengdu, China).

2.2. Preparation of modified MC

The MC was obtained by one-step carbonization-activation method with phosphoric acid and nitrogen doping [19]. The cypress sawdust was sieved and dried at 105°C, and then impregnated by H_3PO_4 for 24 h. After that, the sample was activated under N_2 flow (100 mL/min) at 550°C for 90 min, and washed by hot deionized water (DI) and dried. The obtained MC was immersed in urea solution (1 mol/L) for 24 h, filtered and dried, and then calcined under nitrogen atmosphere at 450°C for 50 min.

5 g MC were added to 50 mL of $Mn(NO_3)_2$ and $Fe(NO_3)_3$ solution (0.09, 0.18, 0.27, 0.36 mol/L), respectively, and then magnetic stirring at 400 rpm for 2 h at room temperature. For Fe–Mn modification, 25 mL of $Fe(NO_3)_3$ solution and 25 mL of $Mn(NO_3)_2$ solution were mixed before MC was added. The concentrations of $Fe(NO_3)_3$ solution were 0.09, 0.18 and 0.27 mol/L. The corresponding concentrations of $Mn(NO_3)_2$ were 0.27, 0.18 and 0.09 mol/L. After impregnating adequately, the samples were filtered and dried at 80°C, and then were heated to 400°C at a rate of 10°C/min under nitrogen atmosphere (with flow rate of 100 mL/min) and held for 2 h. The desired absorbents were named as MC-Fe, MC-Mn and MC-Fe/Mn, respectively.

2.3. Characterization of modified MC

N_2 adsorption/desorption isotherms were carried out using a surface area analyser (ASAP 2460, Micromeritics, USA) at 77 K. The specific surface areas (S_{BET}) of the catalysts were obtained using BET equation. Micropore volume (V_{mic}) and mesopore volume (V_{mes}) were calculated from *t*-plot method and BJH method, respectively. Total pore volume (V_{tot}) was calculated from adsorption amount at the maximum relative pressure.

The functional groups on the surface of the sample were determined by Fourier transform infrared spectrometry (FTIR). The samples were analyzed by infrared spectroscopy using a Nicolet 6700 (Thermo Scientific, USA) infrared spectrometer with scanning range of 4,000–400 cm^{-1}.

X-ray photoelectron spectroscopy (XPS) was measured using an XSAM 800 analyzer (KRATOS, UK) to obtain the information on the elemental composition and the chemical bond state of the samples surface.

Inductively coupled plasma source mass spectrometer (ICP-MS) was conducted using VG PQExCell type mass spectrometer (TJA, USA) to determine the trace metal ions in the solution.

2.4. MB adsorption experiment

0.05 g of the sample was added to a 250 mL Erlenmeyer flask containing 100 mL MB solution at certain concentration,

and then placed in a thermostatic shaker at preset temperature for 60 min with shake. After that the adsorbent was filtrated and the left solution measured by an ultraviolet spectrophotometer at a wavelength of 665 nm. The adsorption amount of MB per unit mass of adsorbent is calculated as follows:

$$q = \frac{(C_0 - C_e) \times V}{M} \quad (1)$$

where q is the adsorption capacity of samples, C_0 and C_e are the initial and equilibrium concentration of MB, respectively, M is the mass of the adsorbent and V is the volume of MB solution.

The kinetic adsorption experiments were carried out in a thermostatic shaker with a rotating speed of 150 rpm at 25°C. The initial concentration of MB was about 500 mg/L and the dosage of the adsorbent was 0.5 g/L. The isothermal adsorption experiments were performed with different initial concentrations of MB (100; 300; 500; 1,000 and 1,500 mg/L).

3. Results and discussion

3.1. Properties of Fe and Mn modified MC

3.1.1. Pore structure

The SEM pictures of the metal modified MC and blank MC (Fig. S1) showed that the surface texture of the MC after Fe and Mn adding did not change evidently compared with blank MC. The nitrogen adsorption/desorption isotherms of all the samples (Fig. S2) had the hysteresis loops due to capillary condensation that occurred in the mesopores, suggesting that all the prepared carbons are typical mesoporous materials. It could be found that the nitrogen adsorption capacity of the modified carbons did not change obviously. The mesopore size distribution of modified MC and blank MC was very similar, showing that the Fe and Mn modification did not significantly change the pore size distribution of the MC. The mesopore size of the modified MC and blank MC was mainly in the range of 2–10 nm, concentrated in 2–4 nm.

From Table 1, it can be seen that blank MC exhibited high S_{BET}, V_{mes} and mesoporous ratios. This could be attributed to phosphoric acid as the activation agent, which could penetrate into the plant cell wall by rapid diffusion, hydrolysis and re-diffusion, and promote or catalyze the hydrolysis, dehydration, aromatization of the carbon precursor [20,21]. Since the cypress sawdust was mainly crystalline cellulose, the activation of the crystalline cellulose produced mixture of pore sizes [20]. As shown in Table 1, the Fe and Mn modified MC had similar S_{BET}, V_{tot}, V_{mes} and mesoporous ratios with blank carbon.

The results show that the pore structure of the Fe and Mn modified MC did not obviously change compared with the blank one. This phenomenon was different from previous studies [12,22]. It was found that the Fe modified carbon caused a significant reduction in the S_{BET} and V_{tot}, from 1,094 m^2/g and 0.47 m^3/g to 543 m^2/g and 0.31 m^3/g, respectively [12]. It was observed a decrease in the S_{BET} and V_{tot} of Mn modified carbon, from 1,220 m^2/g and 1.99 m^3/g to 116 m^2/g and 0.895 m^3/g, respectively [22]. This might result from the pore structure partly blocked by the metal oxides nanoparticles in previous studies. However, in this study, the pore structure of the Fe and Mn modified MC were not reduced obviously. It could be attributed to both the mesoporous carbon structure and the nitrogen-containing functional groups, which could promote the coordination of metal ions, such that the metal oxides particles were uniformly distributed on the surface of the carbon [16–18]. As a result, the agglomeration of the metals and the clogging of the pores were reduced significantly compared with non-mesoporous MC or those without nitrogen-containing functional groups.

3.1.2. Metal phase

The metals were successfully loaded on the surface of the nitrogen doped MC. The relative contents of the metals on the modified MC are shown in Table 2. The results show that the relative contents of Fe on the surface of MC-Fe were 4.4%, while that of the Mn was 3.5% on the MC-Mn, when 0.18 mol/L of $Fe(NO_3)_3$ and $Mn(NO_3)_2$ solution was used to modify MC. The relative contents of Fe on the MC-Fe/Mn were 2.6%, while no Mn was detected, when 0.27 mol/L of

Table 2
Element contents of iron and manganese modified MC (wt.%)

Element	MC	MC-Fe	MC-Mn	MC-Fe/Mn
C	88.3	80.2	82.9	83.7
O	9.9	15.4	13.6	13.7
N	1.8	–	–	–
Fe	–	4.4	–	2.6
Mn	–	–	3.5	–

Table 1
Porous structure of iron and manganese modified MC

Sample	S_{BET} (m^2/g)	S_{ext} (m^2/g)	S_{int} (m^2/g)	V_{tot} (cm^3/g)	V_{mic} (cm^3/g)	V_{mes} (cm^3/g)	V_{mes}/V_{tot}	D_p (nm)
MC	1,214	1,011	203	1.00	0.09	0.91	0.91	3.3
MC-Fe	1,207	962	245	0.98	0.11	0.87	0.89	3.2
MC-Mn	1,201	994	207	0.98	0.10	0.88	0.90	3.2
MC-Fe/Mn	1,194	945	249	0.96	0.11	0.85	0.89	3.2

S_{BET}: BET surface area; S_{ext}: external surface area; S_{int}: internal surface area; V_{tot}: total pores volume; V_{mic}: micropore volume; V_{mes}: mesopore volume; D_p: average pore size.

$Fe(NO_3)_3$ and 0.09 mol/L of $Mn(NO_3)_2$ in mixed solution was used to modify MC. This may be due to the lower concentration of Mn in the mixed solution, and the preferential adsorption of Fe on the MC during the modification process of MC [23,24].

As shown in Fig. 1, a broad XRD peak of carbon was observed obviously on Fe and Mn modified MC, but no diffraction peaks of metals or metal oxides were observed. This indicated that Fe and Mn were loaded in a highly dispersed state on the nitrogen doped MC [25]. It was reported that MC was a potential support to immobilize and disperse Fe [18]. In this study, Fe and Mn could be distributed on the surface of mesoporous carbon uniformly. On the other hand, the introduction of nitrogen on the MC increased the nitrogen-containing functional groups, which could form a coordination compound with metal ions [16,17]. This could promote the uniform dispersion of the metals on the MC and reduces agglomeration [16–18].

3.1.3. Surface chemistry

The FTIR results show that the absorption bands at 3,400; 1,560; 1,452; 1,150; 1,058 and 615 cm^{-1} could be found for all the metals modified MC and blank MC. The infrared peak at 3,400 cm^{-1} can be attributed to the stretching vibration of hydroxyl O–H in H_2O [26]. The infrared peaks at 1,560 and 1,452 cm^{-1} can be assigned to the stretching vibration peak of C=O [27], and the symmetrical bending vibration of $O–CH_3$ [28], respectively, while the peak at 1,150 cm^{-1} is attributed to the C–OH single-bond stretching vibration [29]. The peaks at 1,058 and 615 cm^{-1} can be attributed to the torsional bending vibration of C–OH and C–O–H [24,30], respectively. The results show that the main functional groups on the MC were preserved after the metals modification.

However, it can be clearly observed that the intensity of the symmetrical bending vibration peak of the infrared peak $–O–CH_3$ and C–OH in the MC-Fe were significantly changed with respect to C–O–H, compared with MC. This indicates that the introduction of Fe might promote the formation of $–O–CH_3$ and C–OH on the carbon surface [24,28]. The intensity of C=O infrared peak on MC-Mn was significantly enhanced with respect to C–O–H, compared with MC, indicating that the introduction of Mn maybe has a significant effect on the formation of C=O functional groups [27].

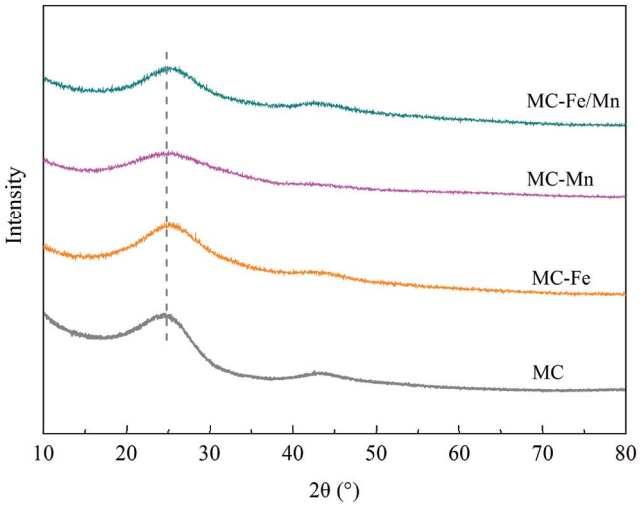

Fig. 1. XRD patterns of iron and manganese modified mesoporous carbon.

As shown in the XPS analysis, the N was successfully doped on the MC (Fig. S3). The N 1s XPS spectrum of the MC shows that there were mainly two types of N in the MC (Fig. S4). The peak at 398.6 eV can be assigned to a pyridine-like N, in which the N atom was bonded to the C atom in sp^2 hybrid form. The peak at 400.2 eV can be assigned to N in the amino or imino group, or N in the pyrrole or pyridone [31]. The nitrogen-containing groups are supposed to be surface coordination sites involved for the adsorption of metal Fe [32]. As shown in Table 2, the relative contents of C, O and N in the blank MC was 88.3%, 9.9% and 1.8%, respectively. However, after the metals loading, the C contents of the modified MC decreased, while those of O increased. This indicates that the addition of metals increased oxygen-containing functional groups on carbon surface, resulting in changed carbon surface chemistry properties. In addition, N was not detected after metals modification, which might be due to the covering of the metals.

The binding energies at 284.6 and 285.8 eV can be assigned to C–C [33,34] and C–O in phenolicether, etc. [35], respectively. Those peaks near 287.8 and 289.8 eV can be attributable to the C=O of carbonyl or benzoquinone [36,37] and delocalized π-electron carbon [38], respectively. The results show that the metal-modified MC had similar surface carbon-containing functional groups (Fig. S6). The binding energy and relative contents of C 1s on the samples are shown in Table 3. Compared with blank MC, the relative contents of C–C on the surface of metal modified MC decreased, while the relative contents of C–O and C=O groups increased slightly. For the MC-Mn and MC- Fe/Mn, the relative contents of C–O, C=O and π–π* were slightly lower than MC-Fe.

3.2. Methylene blue adsorption of modified MC

Table 4 shows the adsorption capacity of modified MC. The maximum adsorption capacity of Fe modified MC was obtained at 933.2 mg/g with 88.1% of removal rate. Compared with that of blank MC, the adsorption amount of MB by Fe-modified MC was higher, indicating that the Fe modification of MC may be beneficial to the adsorption of MB. The MB adsorption capacity of Mn modified MC were significantly higher than blank MC. The MB adsorption capacity of Mn modified MC reached the maximum value at 1,000.5 mg/g with 89.9% of the removal rate. If the Mn ratio was too high, the MC pores may be blocked, and affected their adsorption capacity [39,40]. The adsorption capacity of MB by Fe-Mn modified MC reached 994.6 mg/g, which was better than blank MC.

The three-dimensional structure of MB molecule is about 1.447 nm [41]. MB molecules in aqueous solution often exist as monomers or dimers [42]. Therefore, the mesopore size distribution of the MC favors the MB adsorption. In this study, the pore structure of metals modified MC did not change compared with blank one, and mesopores were retained without clogging after metal modification (Table 1),

Table 3
C 1s binding energy (BE) and relative contents (RCs) of iron and manganese modified MC

Sample	C–C		C–O		C=O		π-π*	
	BE (eV)	RC (%)	BE (eV)	RC (%)	BE (eV)	RC (%)	BE (eV)	RC (%)
MC	284.6	72.8	285.8	14.7	287.5	7.2	289.6	5.4
MC-Fe	284.6	65.4	285.7	18.6	287.6	9.5	289.9	5.5
MC-Mn	284.6	68.7	285.6	17.5	287.4	8.4	289.3	5.4
MC-Fe/Mn	284.6	70.5	285.8	16.2	287.6	8.0	289.8	5.3

Table 4
Adsorption properties of methylene blue by iron and manganese modified MC

		Methylene blue	
Metal	Metal/MC (mol/L)	Adsorption capacity (mg/g)	Removal efficiency (%)
MC	0	854.2	76.8
Fe	0.09	928.7	87.2
	0.18	933.2	88.1
	0.27	908.2	84.9
	0.36	923.6	86.6
Mn	0.09	965.2	86.7
	0.18	1,000.5	89.9
	0.27	956.2	85.5
	0.36	936.4	84.3
Fe + Mn	0.27Fe + 0.09Mn	994.6	89.0
	0.18Fe + 0.18Mn	956.1	86.5
	0.09Fe + 0.27Mn	947.0	85.9

Condition: T = 25°C, C = 556 mg/L, M_{ad} = 0.5 g/L.

which is beneficial for MB adsorption. On the other hand, it was reported that carbonyl groups on MC have the great effect on the adsorption of organic compounds [43]. MB as an electron acceptor, methoxy or carbonyl as an electron donor, could format an electron-acceptor complex [43]. Methoxy and the carbonyl group could promote the adsorption of MB. In this study, the introduction of Mn might cause a change of the carbonyl group and the Fe maybe caused a change of the methoxy group, which would be beneficial for the adsorption of MB.

Based on the above results, the possible adsorption mechanisms for methylene blue by the metals modified N-doping MC could be proposed, as shown in Fig. 2. The blank MC was prepared by one-step carbonization activation using phosphoric acid as activation agent, and then nitrogen-doped MC was obtained by urea modification. The introduction of nitrogen could promote the coordination of metal ions, and thus the metal particles were uniformly distributed on the surface of the carbon, reducing the agglomeration of the metals and the clogging of the pores. The mesoporous structure can remove MB by physical interception. Meanwhile, the introduction of metals resulted in the increase of oxygen-containing groups on carbon. The introduction of Fe could promote the formation of –O–CH_3 and C–OH on the carbon surface, while Mn may have an effect on the formation of C=O functional groups (Table 2). The oxygen-containing (–O–CH_3 and C=O) functional group can adsorb MB by electron donor-receptor action. Thus, the unchanged mesoporous structure, metal active adsorption sites and modified surface chemistry on modified MCs improve the adsorption performance of MB greatly.

3.3. Adsorption kinetics of modified MC

The adsorption of MB on MC in liquid mainly consists of three processes: first, MB could transfer to the surface of MC; second, MB diffuses inside the MC particles; third, MB is adsorbed into the inner surface of pores of MC particles. To better understand the adsorption mechanism and adsorption rate of MB by the three modified MC (MC-Mn, MC-Fe and MC-Fe/Mn), the Weber–Morris intraparticle diffusion model, the pseudo-first-order kinetics and the pseudo-second-order kinetics models were used for fitting experiment data. The three models were expressed by the following:

$$\ln\left(q_e - q_t\right) = \ln q_e - K_1 t \tag{2}$$

where q_e and q_t are the concentrations of adsorption equilibrium and adsorbed at t (min), and K_1 (min^{-1}) is the model constant of the first-order kinetics.

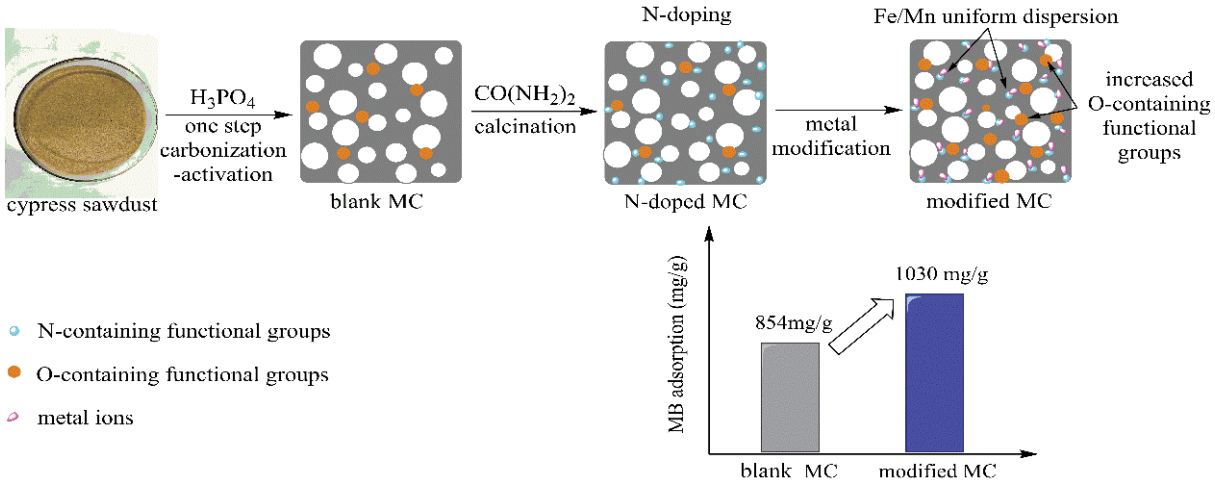

Fig. 2. Proposed adsorption mechanisms for methylene blue by the metals modified N-doping mesoporous carbon from waste biomass.

$$\frac{t}{q_t} = \frac{1}{K_2 q_e^{\,2}} + \frac{1}{q_e} t \tag{3}$$

where K_2 (g/mg min) is the model constant of the pseudo-second-order kinetics.

$$q_t = K_{WM} t^{1/2} + C \tag{4}$$

where K_{WM} (mg/g min$^{0.5}$) is the model constant of the Weber–Morris intraparticle diffusion model.

As shown in Fig. 3, the three modified MC exhibited a rapid uptake of MB at the initial 1 min, which could be due to the excessive porous structure of MC. And then, the adsorption rate decreased gradually, and the adsorption equilibrium was approached at about 60 min. The equilibrium adsorption capacities of MB were in the order of MC-Mn > MC-Fe/Mn > MC-Fe. The results also demonstrated that the introduction of Mn was relatively more beneficial to adsorb MB obviously.

As we can see from the nonlinear fitting curve in Fig. 3, the pseudo-second-order had the highest fit degree. The relevant results of the nonlinear fitted graph are shown in Table 5. The correlation coefficients fitted by the pseudo-second-order kinetic model were all 1.00. Therefore, the pseudo-second-order kinetics was more suitable for describing the adsorption of MB by the three modified MC, and the adsorption process could be controlled by chemical adsorption mechanism [44,45]. This demonstrates the role of surface functional groups in the adsorption of MB by modified MC. Thus, the adsorption process of modified MC to MB includes chemical and physical adsorption. The parameter C signifies the thickness of boundary layer, which is usually applied for evaluating the diffusion resistance [7]. The C value was not 0, indicating that the intraparticle diffusion process was not the only speed-control step [46]. The C_1 values were high, suggesting that their external diffusion resistance was high. The C_2 values were evidently high, indicating that the adsorption achieved equilibrium [7].

3.4. Adsorption isotherms of modified MC

Adsorption isotherms are the curves of the equilibrium adsorption capacity (q_e) and the equilibrium concentration of MB in solution (C_e) during the adsorption of MB by the adsorbent at a constant temperature. At certain temperature, the experimental data are used to fit the adsorption isotherm, which can be used to understand the adsorption amount, adsorption strength and adsorption state of the adsorbent on MB.

Fig. 4 shows the isothermal adsorption curve of modified MC for MB at 25°C. As the initial concentration of MB increased, the equilibrium adsorption capacity was increased. Langmuir, Freundlich and Temkin models were used to fit isothermal adsorption of MB by the three modified MC. The three models were expressed by the following equations:

$$\frac{C_e}{q_e} = \frac{C_e}{q_m} + \frac{1}{K_L q_m} \tag{5}$$

where C_e (mg/L), K_L (L/mg) and q_m (mg/g) were the equilibrium concentration of MB, Langmuir adsorption rate and the adsorption capacity, respectively.

$$\ln q_e = \ln K_F + \frac{1}{n} \ln C_e \tag{6}$$

where K_F ((mg/g)/(L/mg)$^{1/n}$) and n are the adsorption constants of Freundlich.

$$q_e = B \ln A + B \ln C_e \tag{7}$$

where B (J/mol) and A (L/mg) are the correlation constant of the Temkin model.

Fig. 4 shows the non-linear fitting of Langmuir, Freundlich and Temkin models for MB adsorption by modified MC. The parameters are summarized in Table 6. The modified MC q_e increased with C_e and all the three models could provide a good fitting with R^2 higher than 0.95. The correlation

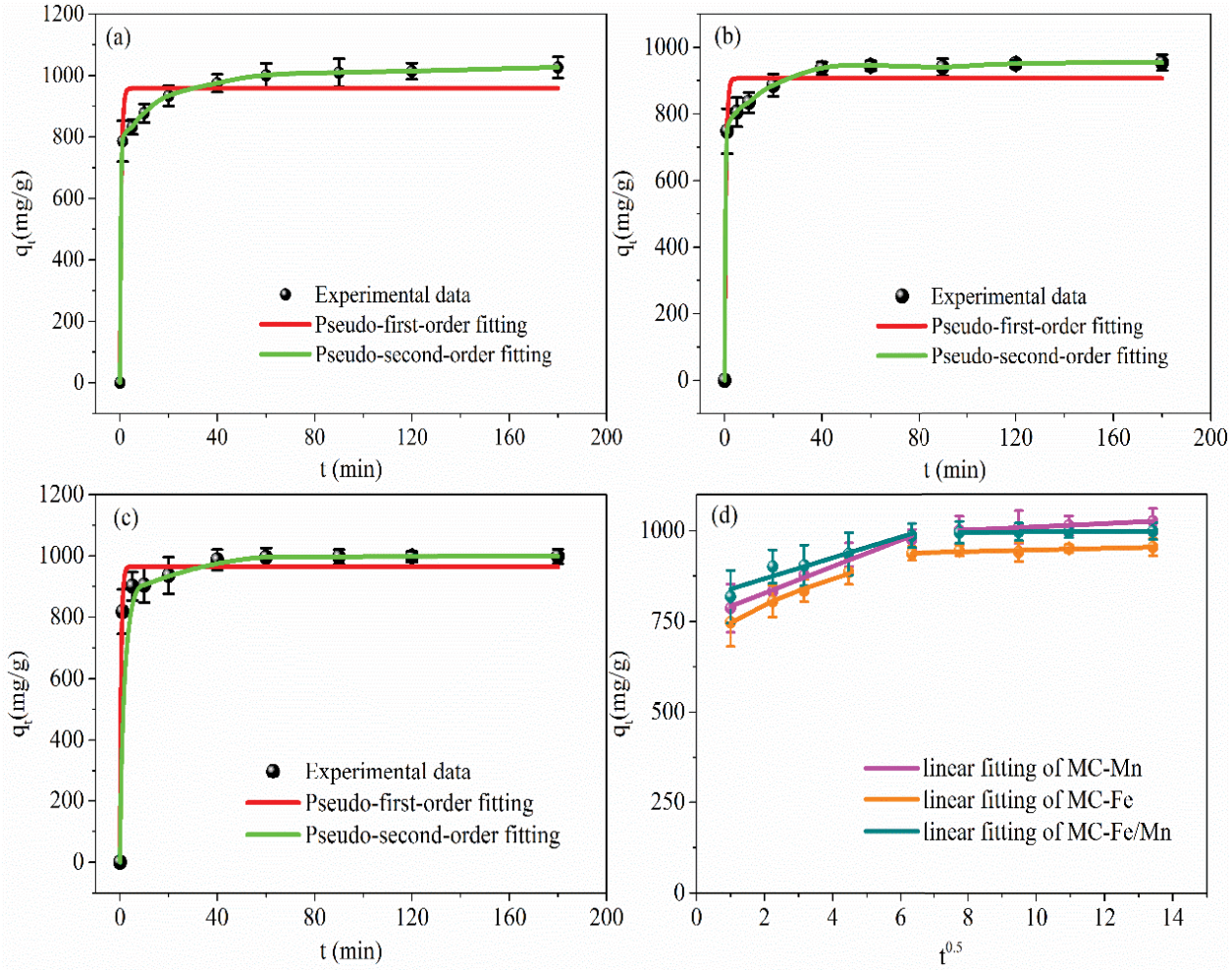

Fig. 3. Non-linear fitting of pseudo-first-order and pseudo-second-order model for methylene blue adsorption by modified MC ((a) MC-Mn, (b) MC-Fe and (c) MC-Fe/Mn), and (d) linear fitting of Weber-Morris intraparticle diffusion model. (Conditions: T = 25°C, C_0 = 572 mg/L, M_{ad} = 0.5 g/L).

Table 5
Kinetic parameters for methylene blue by iron and manganese modified MC

Kinetic model	Fitting parameter	MC-Mn	MC-Fe	MC-Fe/Mn
Pseudo-first-order kinetics	$q_{e,cal}$ (mg/g)	958.3	906.4	964.3
	K_1 (min^{-1})	1.714	1.741	1.883
	R^2	0.953	0.965	0.982
Pseudo-second-order kinetics	$q_{e,cal}$ (mg/g)	1,030.5	958.3	1,002.9
	K_2 (g/(mg min))	6.16×10^{-4}	9.65×10^{-4}	1.36×10^{-3}
	R^2	1.000	1.000	1.000
Weber–Morris intraparticle diffusion model	K_{WM1} (mg/g min$^{0.5}$)	36.55	39.08	28.73
	K_{WM2} (mg/g min$^{0.5}$)	4.39	2.25	0.60
	C_1	755.1	712.12	810.22
	C_2	966.6	923.5	990.49
	R_1^2	0.980	0.996	0.922
	R_2^2	0.996	0.801	0.961

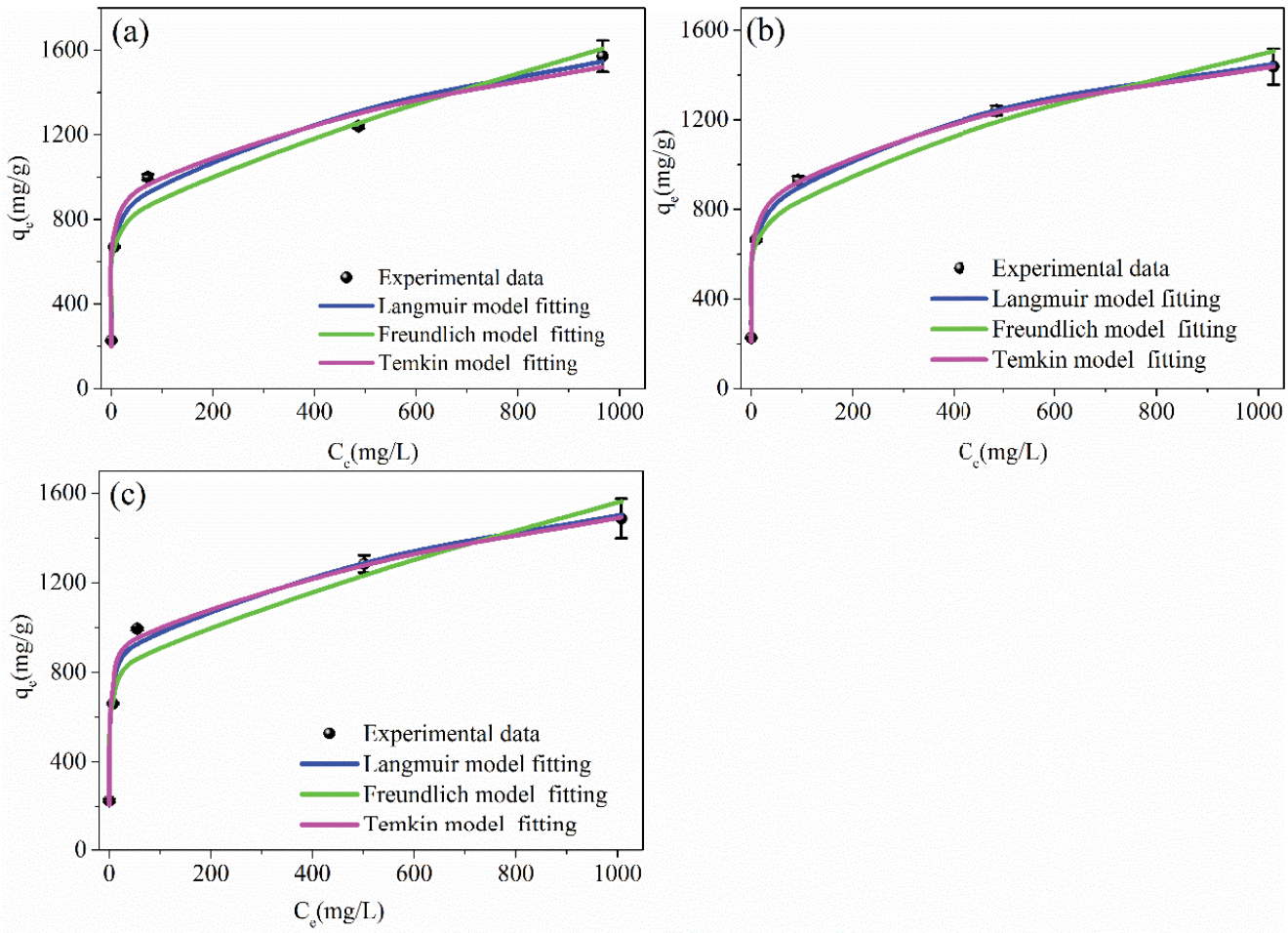

Fig. 4. Non-linear fitting of Langmuir, Freundlich and Temkin model for methylene blue adsorption by modified MC ((a) MC-Mn, (b) MC-Fe and (c) MC-Fe/Mn). (Condition: T = 25°C, t = 60 min, M_{ad} = 0.5 g/L).

Table 6
Isothermal adsorption parameters for methylene blue by iron and manganese modified MC at 25°C

Fitting parameter		MC-Mn	MC-Fe	MC-Fe/Mn
Langmuir	$q_{e,cal}$ (mg/g)	2,248	2,030	2,115
	K_L (mL/mg)	0.0013	0.0014	0.0014
	R^2	0.988	0.996	0.992
Freundlich	K_F ((mg/g)/(L/mg)$^{1/n}$)	28.1	32.0	32.3
	n	1.846	1.940	1.925
	R^2	0.965	0.961	0.953
Temkin	A (L/mg)	0.013	0.014	0.014
	B (J/mol)	5.116	5.519	5.271
	R^2	0.989	0.998	0.994

coefficient R^2 of the Langmuir model fitting was greater than 0.98 which was higher than those of other two models, indicating that the adsorption process of the three modified MC to MB could be mainly uniform monolayer adsorption [47]. The Langmuir model $q_{e,cal}$ was within 2,030–2,248 mg/g, which was much higher than the experimental data (957–1,030 mg/g), indicating that more MB molecules might be adsorbed by optimizing experimental conditions. Meanwhile, the R^2 of Temkin model was also higher than 0.98, suggesting that metal-modified MC has some interaction with MB molecules [48]. The n value was the reciprocal of slope computed from Freundlich at 1.846–1.940, which was greater than 1 and less than 10, indicating that metal-modified MC adsorbs MB easily [49,50].

Table 7
Comparison of adsorption and pore structure onto different adsorbents

Adsorbent	S_{BET} (m^2/g)	V_{tot} (cm^3/g)	D_p (nm)	MB adsorption capacity (mg/g)	Reference
MC	1,214	1.00	3.3	911	This work
MC-Fe	1,207	0.98	3.2	957	This work
MC-Mn	1,201	0.98	3.2	1,030	This work
MC-Fe/Mn	1,194	0.96	3.2	999	This work
AC1	1,094	0.47	1.7	34	[12]
AC1-Fe	543	0.31	2.3	38	[12]
Raw-AC2	912	1.02	5.5	192	[51]
Fe–Ce-AC2	776	0.65	3.4	265	[51]
Raw-AC3	1,094	0.47	3.5	–	[13]
AC3-Fe	544	0.23	5.5	–	[13]
AC4	1,220	1.99	–	–	[22]
AC4-Mn	116	0.90	–	–	[22]

Table 7 shows the comparison of adsorption capacity of MB and pore structure onto different adsorbents. Compared with other adsorbents, the MCs in this study had a higher S_{BET} at about 1,200 m^2/g, and the mesopore ratio was relatively higher at around 90%. In addition, their average pore diameter was small relatively, and thus their adsorption of MB was much higher than the other adsorbents. The rich pores could be attributed to phosphoric acid as the activation agent, which react with carbon to form pores (mainly mesopores) during heating process [20].

As shown in Table 7, activated carbon (AC1/ Raw-AC2/ Raw-AC3/AC4) modified by metals (Fe/Ce/Mn) tends to damage and block pore structure, which would reduce the S_{BET} and V_{tot}, and thus affect the adsorption performance for MB. However, we modified MC with Fe/Mn by nitrogen-doped assistance still have high S_{BET} and V_{tot} compared with MC (Table 1). This indicates that the nitrogen-containing functional groups of MC could complex with metal ions to increase the dispersion of metal particles and reduce the damage to the MC structure. As a result, the original mesoporous structure was maintained largely. Meanwhile, the introduction of metal causes the change of the oxygen-containing functional group (–O–CH_3 and C=O) on the surface of MC (Fig. S5), which was conducive to the adsorption of MB, so that the adsorption performance of MB was significantly improved.

4. Conclusions

The results showed that mesopore structure and nitrogen doping could facilitate uniform dispersion of the metals on carbon, resulting in the unchange of pore structure after metals modification. The introduction of Fe might promote the formation of –O–CH_3, while Mn might have an effect on the formation of C=O functional groups, which would be beneficial for the adsorption of MB. The MB adsorption performance of modified MC increased evidently from 854 to 1,030 mg/g. This could be attributed to unchanged mesoporous structure and change of surface chemistry properties through the introduction of metals. The Langmuir model and pseudo-second-order kinetics were more suitable for describing the adsorption of MB by modified MC, which are mainly uniform monolayer adsorption. The adsorption process was controlled by chemical adsorption, and the metal-modified MC had some interaction with MB molecules.

Acknowledgments

This work is supported by National Natural Science Foundation of China (No. 51778383) and Sichuan Science and Technology Program (2019YFS0500).

References

[1] A. Asghar, A.A. Abdul Raman, W.M.A. Wan Daud, Advanced oxidation processes for in-situ production of hydrogen peroxide/ hydroxyl radical for textile wastewater treatment: a review, J. Cleaner Prod., 87 (2015) 826–838.
[2] M. Cheng, G. Zeng, D. Huang, C. Lai, Z. Wei, N. Li, P. Xu, C. Zhang, Y. Zhu, X. He, Combined biological removal of methylene blue from aqueous solutions using rice straw and *Phanerochaete chrysosporium*, Appl. Microbiol. Biotechnol., 99 (2015) 5247–5256.
[3] F. Ferrero, TOC removal from Methylene Blue aqueous solutions by adsorption and oxidation in the presence of coal fly ash, Desal. Wat. Treat., 57 (2015) 1–5.
[4] V.J.P. Vilar, C.M.S. Botelho, R.A.R. Boaventura, Methylene blue adsorption by algal biomass based materials: biosorbents characterization and process behaviour, J. Hazard. Mater., 147 (2007) 120–132.
[5] N.N. Nassar, A. Ringsred, Rapid adsorption of methylene blue from aqueous solutions by goethite nanoadsorbents, Environ. Eng. Sci., 29 (2010) 790–797.
[6] S.-J. Park, Y.-S. Jang, Pore structure and surface properties of chemically modified activated carbons for adsorption mechanism and rate of Cr(VI), J. Colloid Interface Sci., 249 (2002) 458–463.
[7] Q. Zhou, X. Jiang, Y. Guo, G. Zhang, W. Jiang, An ultra-high surface area mesoporous carbon prepared by a novel MnO-templated method for highly effective adsorption of methylene blue, Chemosphere, 201 (2018) 519–529.
[8] T.Y. Ma, L. Liu, Z.Y. Yuan, Direct synthesis of ordered mesoporous carbons, Chem. Soc. Rev., 42 (2013) 3977–4003.
[9] S. Tanaka, N. Nakatani, A. Doi, Y. Miyake, Preparation of ordered mesoporous carbon membranes by a soft-templating method, Carbon, 49 (2011) 3184–3189.

[10] A. Shukla, Y.-H. Zhang, P. Dubey, J.L. Margrave, S.S. Shukla, The role of sawdust in the removal of unwanted materials from water, J. Hazard. Mater., 95 (2002) 137–152.
[11] M. Hata, Y. Amano, M. Aikawa, M. Machida, F. Imazeki, Preparation of bamboo-based mesoporous activated carbon by phosphoric acid activation, Carbon, 72 (2014) 429–430.
[12] I. Shah, R. Adnan, S.W.N. Wan, N. Mohamed, Iron impregnated activated carbon as an efficient adsorbent for the removal of methylene blue: regeneration and kinetics studies, PLoS One, 10 (2015) e0122603.
[13] I. Shah, R. Adnan, W.S. Wan Ngah, N. Mohamed, Iron impregnated carbon materials with improved physicochemical characteristics, Mater. Sci. Eng B-Adv., 201 (2015) 1–12.
[14] S. Naeem, V. Baheti, J. Militky, J. Wiener, P. Behera, A. Ashraf, Sorption properties of iron impregnated activated carbon web for removal of methylene blue from aqueous media, Fiber Polym., 17 (2016) 1245–1255.
[15] I. Shah, R. Adnan, W.S. Wan Ngah, N. Mohamed, Y.H. Taufiq-Yap, A new insight to the physical interpretation of activated carbon and iron doped carbon material: sorption affinity towards organic dye, Bioresour. Technol., 160 (2014) 52–56.
[16] L. Huang, M. He, B. Chen, Q. Cheng, B. Hu, Highly efficient magnetic nitrogen-doped porous carbon prepared by one-step carbonization strategy for Hg^{2+} removal from water, ACS Appl. Mater. Interaces, 9 (2017) 2550–2559.
[17] S.-M. Alatalo, F. Pileidis, E. Mäkilä, M. Sevilla, E. Repo, J. Salonen, M. Sillanpää, M.-M. Titirici, Versatile cellulose-based carbon aerogel for the removal of both cationic and anionic metal contaminants from water, ACS Appl. Mater. Interfaces, 7 (2015) 25875–25883.
[18] X. Jiang, Y. Guo, L. Zhang, W. Jiang, R. Xie, Catalytic degradation of tetracycline hydrochloride by persulfate activated with nano Fe^0 immobilized mesoporous carbon, Chem. Eng. J., 341 (2018) 392–401.
[19] M. Wang, R. Xie, Y. Chen, X. Pu, W. Jiang, L. Yao, A novel mesoporous zeolite-activated carbon composite as an effective adsorbent for removal of ammonia-nitrogen and methylene blue from aqueous solution, Bioresour. Technol., 268 (2018) 726–732.
[20] M. Jagtoyen, F. Derbyshire, Activated carbons from yellow poplar and white oak by H_3PO_4 activation, Carbon, 36 (1998) 1085–1097.
[21] N.V. Sych, S.I. Trofymenko, O.I. Poddubnaya, M.M. Tsyba, V.I. Sapsay, D.O. Klymchuk, A.M. Puziy, Porous structure and surface chemistry of phosphoric acid activated carbon from corncob, Appl. Surf. Sci., 261 (2012) 75–82.
[22] E. Pargoletti, V. Pifferi, L. Falciola, G. Facchinetti, A. Re Depaolini, E. Davoli, M. Marelli, G. Cappelletti, A detailed investigation of MnO_2 nanorods to be grown onto activated carbon. High efficiency towards aqueous methyl orange adsorption/degradation, Appl. Surf. Sci., 472 (2019) 118–126.
[23] M. Guo, G. Qiu, W. Song, Poultry litter-based activated carbon for removing heavy metal ions in water, Waste Manage. (Oxford), 30 (2010) 308–315.
[24] E.R. Valinurova, A.D. Kadyrova, L.R. Sharafieva, F.K. Kudasheva, Use of activated carbon materials for wastewater treatment to remove Ni(II), Co(II), and Cu(II) ions, Russ. J. Appl. Chem., 81 (2008) 1939–1941.
[25] S.-F. Lo, S.-Y. Wang, M.-J. Tsai, L.-D. Lin, Adsorption capacity and removal efficiency of heavy metal ions by Moso and Ma bamboo activated carbons, Chem. Eng. Res. Des., 90 (2012) 1397–1406.
[26] Y.B. Tang, Q. Liu, F.Y. Chen, Preparation and characterization of activated carbon from waste ramulus mori, Chem. Eng. J., 203 (2012) 19–24.
[27] K.C. Bedin, A.C. Martins, A.L. Cazetta, O. Pezoti, V.C. Almeida, KOH-activated carbon prepared from sucrose spherical carbon: adsorption equilibrium, kinetic and thermodynamic studies for methylene blue removal, Chem. Eng. J., 286 (2016) 476–484.
[28] A.B. Albadarin, M.N. Collins, M. Naushad, S. Shirazian, G. Walker, C. Mangwandi, Activated lignin-chitosan extruded blends for efficient adsorption of methylene blue, Chem. Eng. J., 307 (2017) 264–272.
[29] M. Li, W. Li, S. Liu, Hydrothermal synthesis, characterization, and KOH activation of carbon spheres from glucose, Carbohydr. Res., 346 (2011) 999–1004.
[30] P.S. Kumar, T. Prot, L. Korving, K.J. Keesman, I. Dugulan, M.C.M.V. Loosdrecht, G.J. Witkamp, Effect of pore size distribution on iron oxide coated granular activated carbons for phosphate adsorption – importance of mesopores, Chem. Eng. J., 326 (2017) 231–239.
[31] O.S.G.P. Soares, R.P. Rocha, A.G. Gonçalves, J.L. Figueiredo, J.J.M. Órfão, M.F.R. Pereira, Easy method to prepare N-doped carbon nanotubes by ball milling, Carbon, 91 (2015) 114–121.
[32] Y.F. Jia, B. Xiao, K.M. Thomas, Adsorption of metal ions on nitrogen surface functional groups in activated carbons, Langmuir, 18 (2002) 470–478.
[33] H. Liu, G. Li, C. Hu, Selective ring CH bonds activation of toluene over Fe/activated carbon catalyst, J. Mol. Catal. A: Chem., 377 (2013) 143–153.
[34] K. Li, L. Ling, C. Lu, W. Qiao, Z. Liu, L. Liu, I. Mochida, Catalytic removal of SO_2 over ammonia-activated carbon fibers, Carbon, 39 (2001) 1803–1808.
[35] Z.R. Yue, W. Jiang, L. Wang, S.D. Gardner, C.U.P. Jr, Surface characterization of electrochemically oxidized carbon fibers, Carbon, 37 (1999) 1785–1796.
[36] Y.-W. Lee, H.-J. Kim, J.-W. Park, B.-U. Choi, D.-K. Choi, J.-W. Park, Adsorption and reaction behavior for the simultaneous adsorption of NO–NO_2 and SO_2 on activated carbon impregnated with KOH, Carbon, 41 (2003) 1881–1888.
[37] M. Bastos-Neto, D.V. Canabrava, A.E.B. Torres, E. Rodriguez-Castellón, A. Jiménez-López, D.C.S. Azevedo, C.L. Cavalcante, Effects of textural and surface characteristics of microporous activated carbons on the methane adsorption capacity at high pressures, Appl. Surf. Sci., 253 (2007) 5721–5725.
[38] H. Guedidi, L. Reinert, J.M. Lévêque, Y. Soneda, N. Bellakhal, L. Duclaux, The effects of the surface oxidation of activated carbon, the solution pH and the temperature on adsorption of ibuprofen, Carbon, 54 (2013) 432–443.
[39] D. Sinha, R. Maitra, D. Mukherjee, Generalized antisymmetric ordered products, generalized normal ordered products, ordered and ordinary cumulants and their use in many electron correlation problem, Comput. Theor. Chem., 1003 (2013) 62–70.
[40] S. Jiang, L. Zhang, T. Chen, G. Wang, Adsorption separation of vinyl chloride and acetylene on activated carbon modified by metal ions, J. Ind. Eng. Chem., 20 (2014) 1693–1696.
[41] G.L. Dotto, J.M.N. Santos, I.L. Rodrigues, R. Rosa, F.A. Pavan, E.C. Lima, Adsorption of methylene blue by ultrasonic surface modified chitin, J. Colloid Interface Sci., 446 (2015) 133–140.
[42] K. Fujita, K. Taniguchi, H. Ohno, Dynamic analysis of aggregation of methylene blue with polarized optical waveguide spectroscopy, Talanta, 65 (2005) 1066–1070.
[43] J.A. Mattson, H.B.M. Jr, M.D. Malbin, W.J.W. Jr, J.C. Crittenden, Surface chemistry of active carbon: Specific adsorption of phenols, J. Colloid Interface Sci., 31 (1969) 116–130.
[44] C. Zhang, Y. Wang, X. Yan, Liquid-phase adsorption: Characterization and use of activated carbon prepared from diosgenin production residue, Colloids Surf.. A, 280 (2006) 9–16.
[45] X. Peng, M. Wang, F. Hu, F. Qiu, H. Dai, Z. Cao, Facile fabrication of hollow biochar carbon-doped TiO_2/CuO composites for the photocatalytic degradation of ammonia nitrogen from aqueous solution, J. Alloys Compd., 770 (2019) 1055–1063.
[46] W.A. Khanday, F. Marrakchi, M. Asif, B.H. Hameed, Mesoporous zeolite–activated carbon composite from oil palm ash as an effective adsorbent for methylene blue, J. Taiwan Inst. Chem. Eng., 70 (2016) 32–41.
[47] A.L. Cazetta, A.M.M. Vargas, E.M. Nogami, M.H. Kunita, M.R. Guilherme, A.C. Martins, T.L. Silva, J.C.G. Moraes, V.C. Almeida, NaOH-activated carbon of high surface area produced from coconut shell: kinetics and equilibrium studies from the methylene blue adsorption, Chem. Eng. J., 174 (2011) 117–125.

[48] E.A. Dil, M. Ghaedi, A. Asfaram, The performance of nanorods material as adsorbent for removal of azo dyes and heavy metal ions: application of ultrasound wave, optimization and modeling, Ultrason. Sonochem., 34 (2017) 792.
[49] B.K. Sen, D.K. Deshmukh, M.K. Deb, D. Verma, J. Pal, Removal of phenolic compounds from aqueous phase by adsorption onto polymer supported iron nanoparticles, Bull. Environ. Contam. Toxicol., 93 (2014) 549–554.
[50] X. Peng, F. Hu, T. Zhang, F. Qiu, H. Dai, Amine-functionalized magnetic bamboo-based activated carbon adsorptive removal of ciprofloxacin and norfloxacin: a batch and fixed-bed column study, Bioresour. Technol., 249 (2018) 924–934.
51. S. Cheng, L. Zhang, A. Ma, H. Xia, J. Peng, C. Li, J. Shu, Comparison of activated carbon and iron/cerium modified activated carbon to remove methylene blue from wastewater, J. Environ. Sci-China., 65 (2018) 92–102.

Supplementary information:

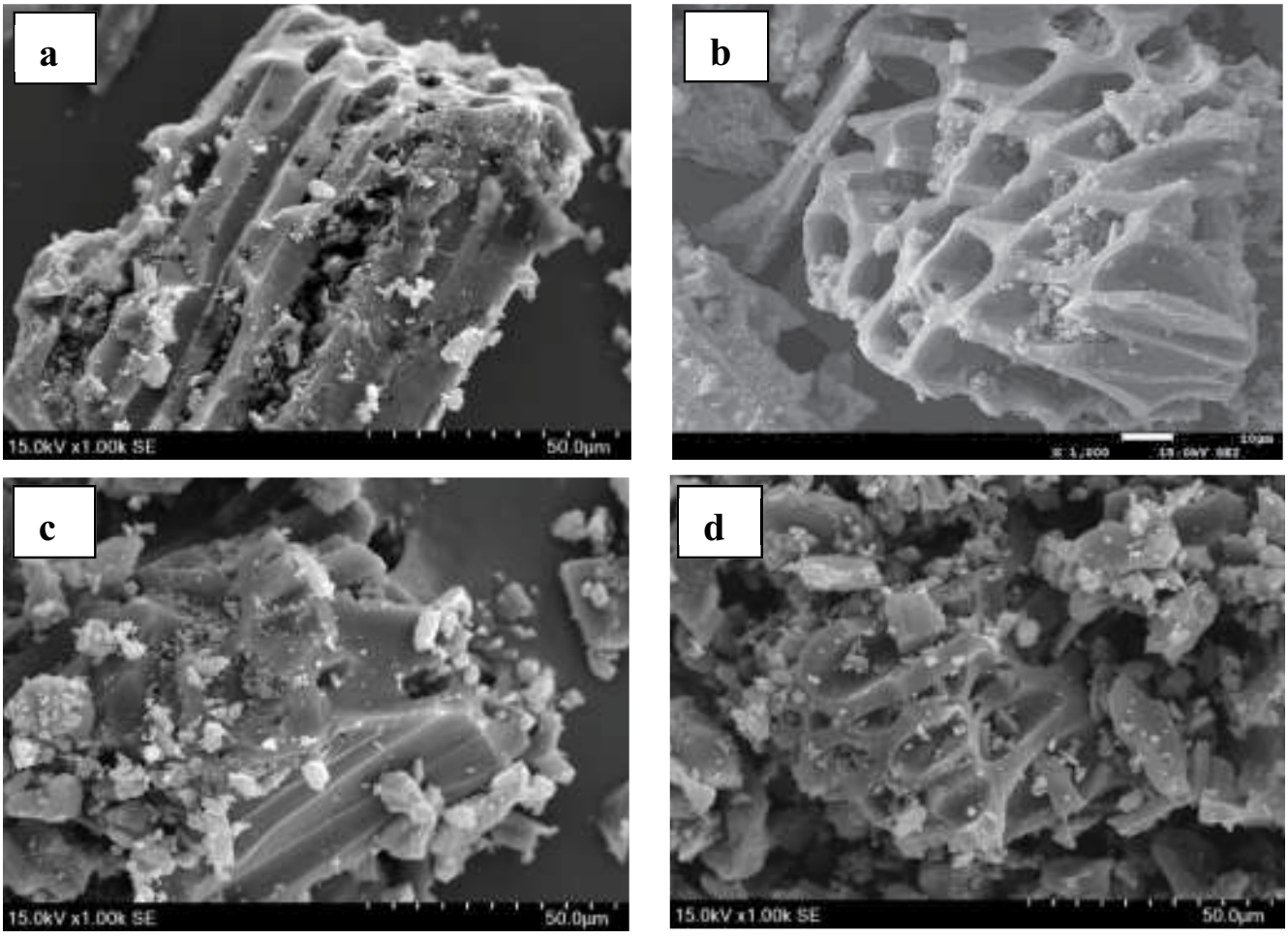

Fig. S1. SEM images of iron and manganese modified MC ((a) MC, (b) MC-Fe, (c) MC-Mn, (d) MC-Fe/Mn).

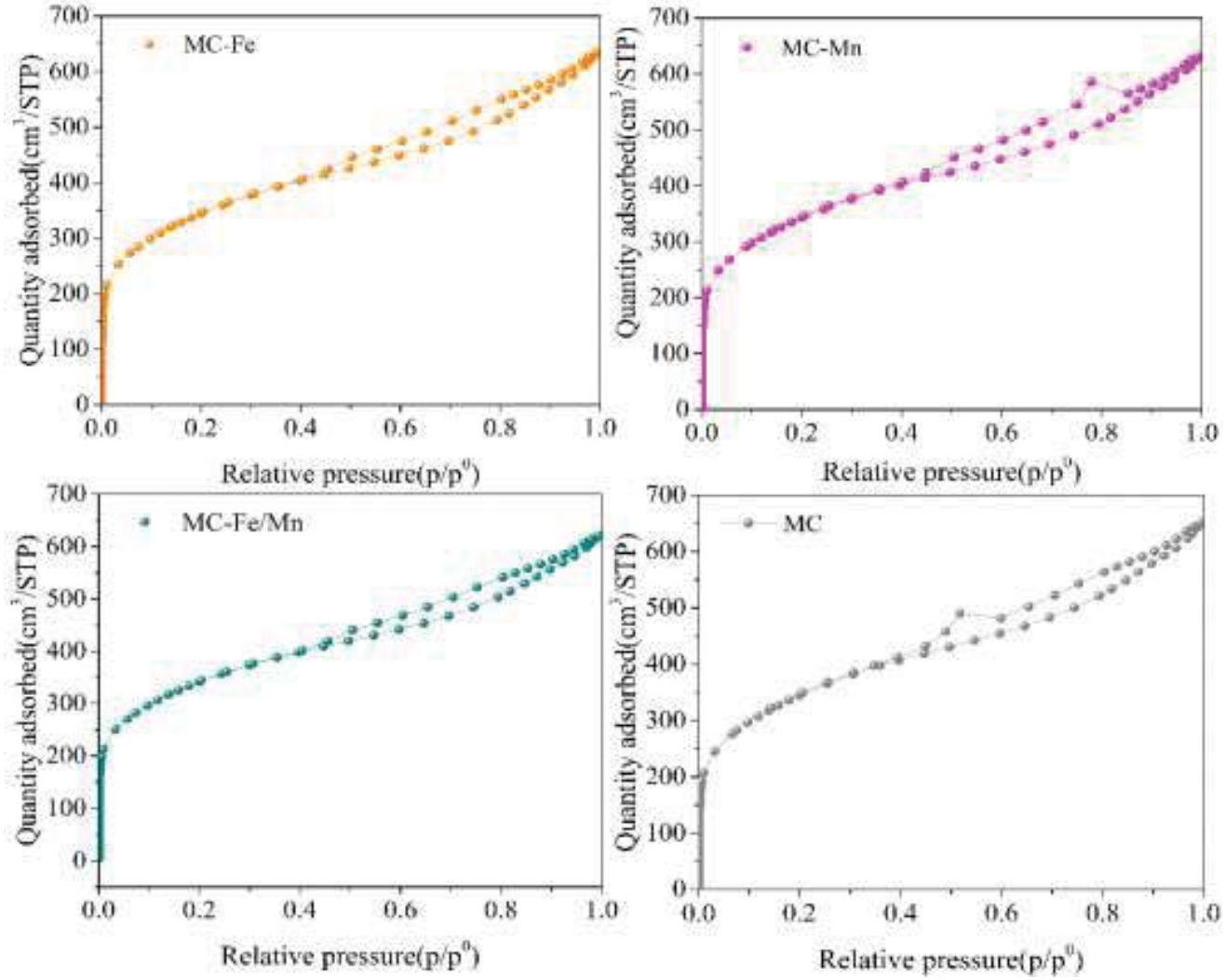

Fig. S2. Nitrogen adsorption/desorption isotherms of iron and manganese modified MC.

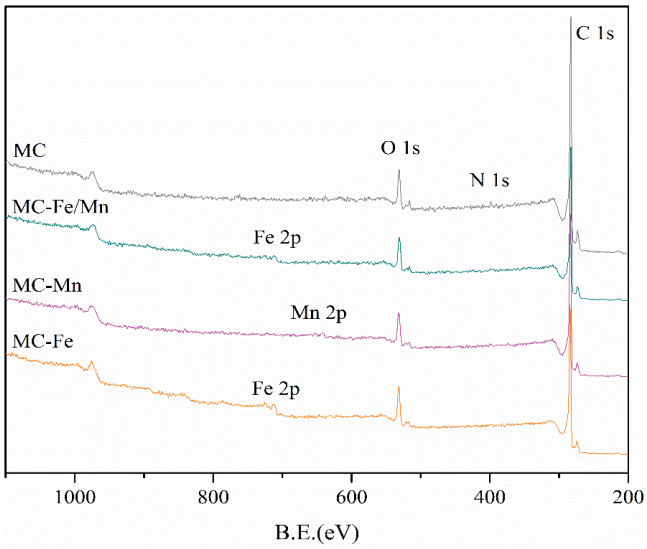

Fig. S3. XPS wide scan spectrum of iron and manganese modified MC.

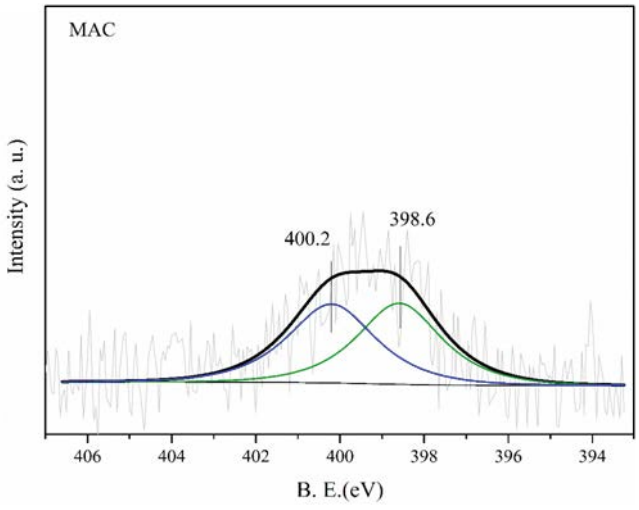

Fig. S4. N 1s spectrum of blank MC.

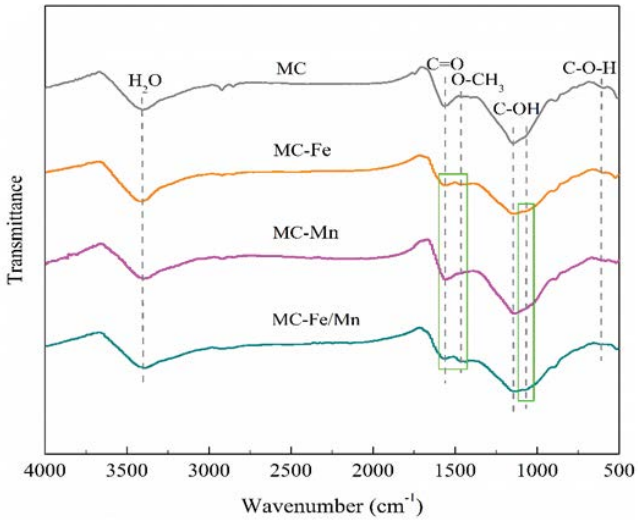

Fig. S5. FTIR of iron and manganese modified MC.

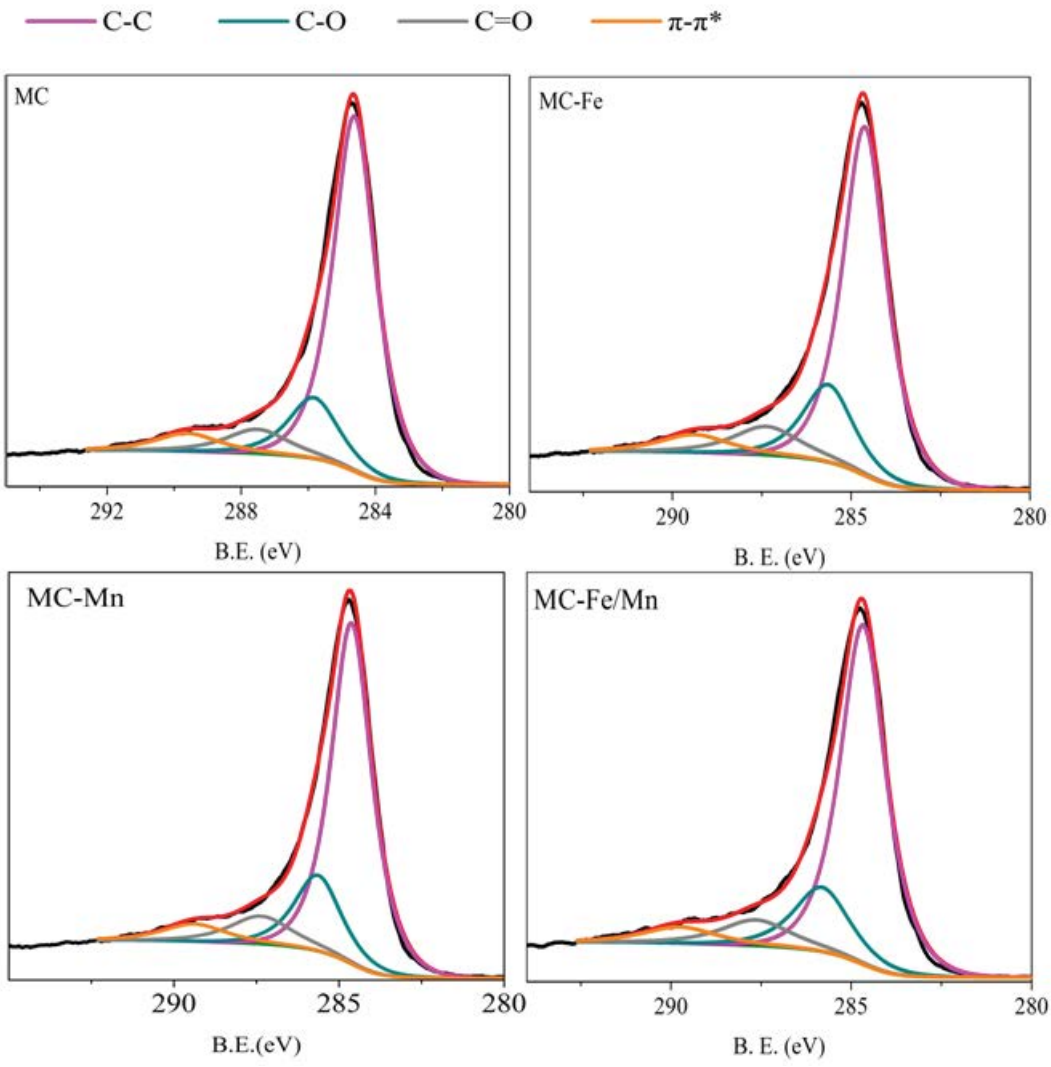

Fig. S6. C 1s spectrum of iron and manganese modified MC.